Nano Communication Networks 8 (2016) 25–34

Contents lists available at ScienceDirect

Nano Communication Networks

journal homepage: www.elsevier.com/locate/nanocomnet

A statistical model for the MIMO channel with rough reflection surfaces in the THz band

Zheng Xu *, Xiaodai Dong, Jens Bornemann

Department of Electrical and Computer Engineering, University of Victoria, EOW448, 3800 Finnerty Rd, Victoria, V8P 5C2, Canada

ARTICLE INFO

Article history:
Received 31 May 2015
Received in revised form 25 September 2015
Accepted 26 September 2015
Available online 3 November 2015

Keywords:
Terahertz communication
MIMO system
Channel capacity
Rough surface scattering

ABSTRACT

Based on the reflection properties of rough surfaces, we propose a statistical multiple-input multiple-output (MIMO) antenna system in the terahertz (THz) band for nanocommunications. Firstly, our analysis of scattering from a rough surface indicates that the reflection from a single surface can be a cluster of rays. Secondly, a new MIMO model for THz communications is proposed. In this model, the number of multipaths is highly dependent on the roughness of the reflecting surfaces. When the surface is ideally smooth, the MIMO channel is sparse and as a result, the capacity is sub-linear with the MIMO scale. On the other hand, when the surface is rough, more degrees of freedom are provided by the scattered rays. Finally, channel capacities with different surface roughness are numerically calculated and compared between different MIMO scales. The results show that in contrast to the GHz range, large scale THz multiple antennas may not provide as much multiplexing gain. Therefore, it is necessary to determine the antenna scale according to the actual propagation environment.

1. Introduction

The THz band (0.1–10 THz) is one of the most promising bands that will satisfy the demand for higher data rates in wireless communications. It has been shown that about 47 GHz of unregulated bandwidth is available around 350 GHz with low atmospheric absorption [1], and that for short transmission distances, the capacity can even be higher than 1 Tbit/s when the frequency is over 1 THz. When the frequency increases and the devices size scales down, wireless communications will fall into the range of nano-scale communications. Recently, many nano-scale devices have been designed for nanocommunications in the THz band, such as graphene based nano transceivers [2] and antennas [3–9]. Some nanocommunication THz channel models have been proposed in the literature. For example, paper [10] analyzes the capacity of a THz channel. Papers [11–14] review the background knowledge and recent research progress in THz technology, and they reveal that some electrical components for THz frequencies are already commercially available.

On the other hand, the multiple-input multiple-output (MIMO) antenna technique is well known to increase the data rate of a wireless communication system [15]. MIMO theory and precoding schemes in the GHz band have already been well presented in the literature. In a GHz channel, it is usually assumed that the elements of a fading channel matrix **H** are independent and identically distributed (i.i.d.), which is based on the assumption of a rich scattering environment that has many multipaths. Under this assumption, the physical channel can be viewed as several parallel sub-channels, and the total capacity scales up linearly with the MIMO dimension. However, for some scenarios in the THz channel and with increasing MIMO dimension, MIMO systems show only beamforming gain but limited multiplexing gain improvement. This is due to the fact that the number of multipaths in the THz channel is limited since the path loss and reflection loss are so

* Corresponding author. Tel.: +1 250 891 3765.
E-mail addresses: zhengxu@ece.uvic.ca (Z. Xu), xdong@ece.uvic.ca (X. Dong), jbornema@ece.uvic.ca (J. Bornemann).

http://dx.doi.org/10.1016/j.nancom.2015.09.002
1878-7789/

large that only the single bounce reflection rays are strong enough to link transmitters with receivers. Therefore, the models of the GHz channel cannot directly be applied to the THz channel, and new models for THz MIMO systems must be developed. It is generally agreed that THz MIMO systems have the following characteristics: (i) The scenarios are mainly applied to indoor environments, for example, office buildings or malls [11]. For long distance outdoor communications, smart antennas with high power amplifiers must be applied [1]; (ii) For indoor THz MIMO channels, few multipaths exist between the transmitting and receiving antennas if all the surfaces are smooth [16,17]. The correlations between the received signals on different receive antennas are significantly higher than those in the GHz band. Therefore, the multiplexing gain will be low, and correlated signals have low diversity gain. This situation is very similar to the sparse MIMO channel that has been studied in some theoretical investigations [18,19] as well as in experiments [20].

Most of the existing works on MIMO system models are in the GHz band, but very few papers study THz MIMO systems. Therefore, in this work, we study MIMO channel modeling for THz communications. Besides the different path loss factors, surface roughness is one of the most important differences between THz and GHz MIMO channels. For THz MIMO models, scattering analysis is far more important than in the GHz range. In [1,16,17,21–23], the scattering from rough surfaces is studied for THz channels. When the carrier frequency is very high, the surfaces of reflecting objects can no longer be regarded as smooth. For THz frequencies, the surfaces of indoor objects, such as wallpaper or carpet, are all sufficiently rough such that their scattering cannot be ignored. The authors of [16,23] studied the scattering power from different reflection angles at 300 GHz and measured the multipath loss in an indoor scenario. We use the same method to investigate the reflection properties of THz frequencies and derive a new MIMO model for indoor nanocommunications. In this new model, the scattered rays are included and become increasingly important with rising frequency. When the frequency is high enough, the specular reflection is less dominant and becomes an ordinary ray with very low power gain. In the capacity analysis, we express the channel capacity as the sum of two parts, one is the capacity introduced by specular reflection, the other one is introduced by scattered rays. Since the specular reflection rays are weak in the THz band, the capacity is mainly contributed by scattered rays. Another very important difference between THz MIMO and GHz MIMO systems is that the antenna size is much smaller in the THz regime and, therefore, we can place hundreds of antennas on a single device, which necessitates the performance analysis of very large scale antenna arrays.

The main contributions of our new THz MIMO model are summarized as follows:

- We propose a THz MIMO system model based on the theory of rough surface reflection and point out the importance of rough surfaces to THz MIMO systems.
- We analyze the relationship between the capacity and the roughness factor, as well as the capacities introduced by different rays.

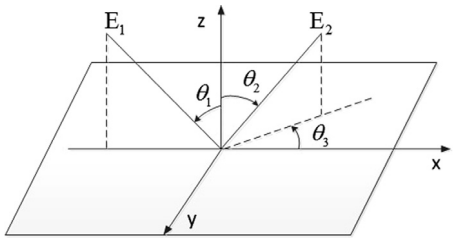

Fig. 1. The scattering reflection geometry.

- We compare the spectral efficiency of systems with different numbers of antennas and in environments with different roughness factors. From this comparisons, it can be determined whether the use multiple antennas is necessary, and if so, how many antennas to employ in the THz band. In addition, the tradeoff between costs and gains under different roughness scenarios can be assessed.

The remainder of this paper is organized as follows: In Section 2, we provide the background on reflections from small-size to large-size rough surfaces. In Section 3, we model the MIMO system in the THz band and analyze the channel capacity of the MIMO system. The simulation results and data analyses are provided in Section 4. Finally, our conclusions are given in Section 5.

2. Reflection in the THz band

2.1. Scattering from a small rough surface

Reflections in the GHz band are typically viewed as being generated by a smooth surface. Under this situation, only the specular reflection ray is considered and the reflection loss is usually ignored. However, there is growing experimental evidence indicating that this is not the case for the THz band. C. Jansen et al. measured the roughness of some common indoor materials, such as plaster and wallpaper [23]. Their results show that the standard deviation of the surface height is about $\sigma_h = 88$ μm for plaster, and $\sigma_h = 90$ μm for wallpaper. Compared with the wavelength at GHz frequencies (e.g., 300 mm at 1 GHz), these surface height deviations are rather small and can be safely ignored. For THz frequencies, however, the wavelength is in the order of several hundred micrometers, which is comparable with the surface height deviation. In such a situation, we must take the roughness into consideration and use a new method to model the reflection properties.

Suppose the incident field $\mathbf{E}_1$ is a harmonic plane wave of unit amplitude. We denote the angle of incidence (the angle between $\mathbf{E}_1$ and the $\mathbf{z}$ axis) as θ_1 and the angles of reflection (the angles between the reflected field $\mathbf{E}_2$ and the $\mathbf{z}$ and $\mathbf{x}$ axes) as θ_2 and θ_3, respectively (Fig. 1). Let $\mathbf{P}$ be the point of observation and r the distance from $\mathbf{P}$ to a point (x, y) on the reflection surface. The scattered field $\mathbf{E}_2$ is given by the Helmholtz integral [24]

$$\mathbf{E}_2(P) = \frac{1}{4\pi} \iint_S \left(\mathbf{E}_1 \frac{\partial \psi}{\partial \mathbf{n}} - \psi \frac{\partial \mathbf{E}_1}{\partial \mathbf{n}} \right) \mathrm{d}S, \tag{1}$$

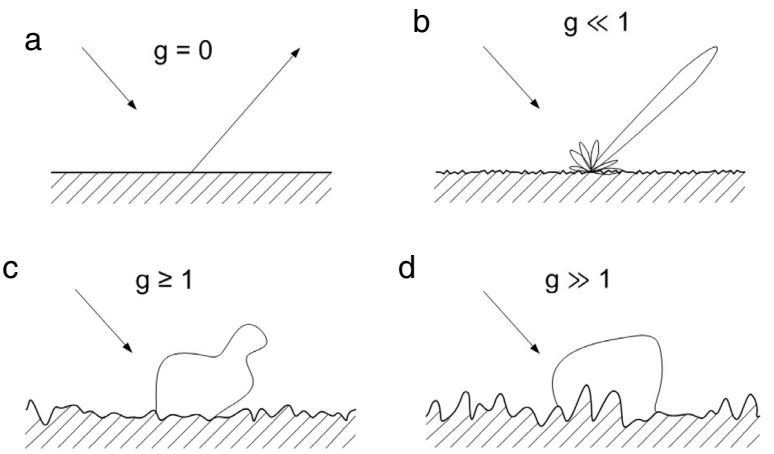

Fig. 2. Transition from specular reflection to diffuse scattering. The surfaces are: (a) smooth, (b) slightly rough, (c) moderately rough, and (d) very rough. *Source:* Data from [24].

where S is the reflection surface, $\mathbf{n}$ is a vector normal to the surface, and ψ is a continuous scalar function denoted as

$$\psi = \frac{e^{ik_2 r}}{r} \tag{2}$$

where k_2 is the wavenumber of the reflected wave. The scattering coefficient ρ is defined as

$$\rho(\theta_1, \theta_2, \theta_3) = \frac{E_2}{E_{sr}}, \tag{3}$$

where E_2 is the amplitude of $\mathbf{E}_2$, and E_{sr} is the field specularly reflected by a smooth and ideally conducting surface.

For a rectangular surface with random height and area of $A = l_x l_y$, the average scattering power coefficient is expressed as [24]

$$\langle \rho \rho^* \rangle = e^{-g}\rho_0 + \frac{\pi T^2 F^2 e^{-g}}{A} \sum_{m=1}^{\infty} \frac{g^m}{m!m} e^{-v_{xy}^2 T^2/4m}. \tag{4}$$

Eq. (4) consists of two terms: the first term corresponds to the specular reflection, and the second term corresponds to the scattered field. When the reflection surface becomes rougher, the significance of the second term increases. For Eq. (4), $k = \frac{2\pi}{\lambda}$ is the wavenumber, T is the surface correlation length, ρ_0 is the scattering coefficient of a plain surface of area A, g is the Rayleigh roughness factor, and v_x, v_y, v_{xy}, and F are notations used to simplify the expression of Eq. (4). These symbols are given by

$$v_x = k(\sin(\theta_1) - \sin(\theta_2)\cos(\theta_3)), \tag{5}$$

$$v_y = k(-\sin(\theta_2)\sin(\theta_3)), \tag{6}$$

$$v_{xy} = \sqrt{v_x^2 + v_y^2}, \tag{7}$$

$$\rho_0 = \mathrm{sinc}(v_x l_x)\mathrm{sinc}(v_y l_y), \tag{8}$$

$$g = k^2 \sigma_h^2 (\cos(\theta_1) + \cos(\theta_2))^2, \tag{9}$$

and

$$F = \frac{1 + \cos(\theta_1)\cos(\theta_2) - \sin(\theta_1)\sin(\theta_2)\cos(\theta_3)}{\cos(\theta_1)(\cos(\theta_1) + \cos(\theta_2))}. \tag{10}$$

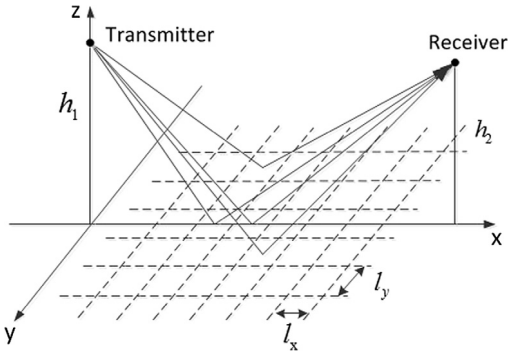

Fig. 3. The large surface is divided into many small sub-tiles.

It is evident from Eq. (9) that the roughness factor g is dependent on frequency, the surface derivation, the incident angle θ_1 and the angle of reflection θ_2. Fig. 2 shows the reflection patterns of different roughnesses, from a smooth surface ($g = 0$) to a very rough surface ($g \gg 1$).

2.2. Scattering from a large rough surface

The discussion in the previous section holds only when the surface area A is small. When the dimensions of the reflecting surface are comparable with the distance between the transmitter and receiver, the total field at $\mathbf{P}$ is the accumulation of many rays with different angles of reflection. Therefore, treating the surface as a single tile and using a single angle of reflection will introduce tremendous error. To remedy this situation, we use the method presented in [21] and divide the surface into small sub-tiles.

Suppose the surface is in the x–y plane, the transmitter is on the z axis, and the receiver is in the x–z plane, as shown in Fig. 3. The entire surface is divided into many sub-tiles of the same size. Each sub-tile has its own incident/reflection angles which can be obtained by geometrical calculations. The scattering coefficient using sub-tiles is shown in Fig. 4. Note that the amplitude of each sub-tile is highly correlated with the size of the sub-tile. If

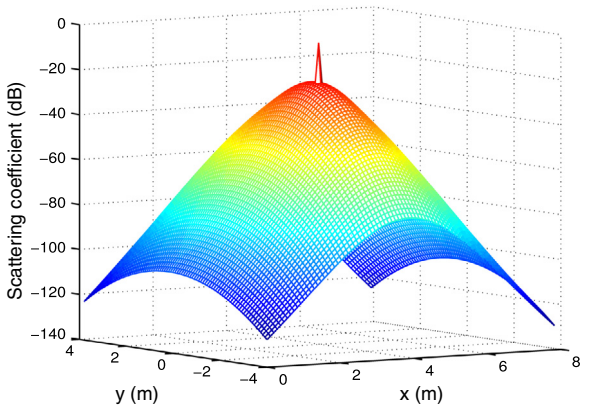

Fig. 4. The scattering coefficient of a rough surface. The positions of the transmitter and receiver are (0, 0, 4) and (8, 0, 4) respectively. The frequency is 300 GHz, $T = 2.3$ mm, $l_x = l_y = 40$ T, and $\sigma_h = 0.13$ mm [21,22].

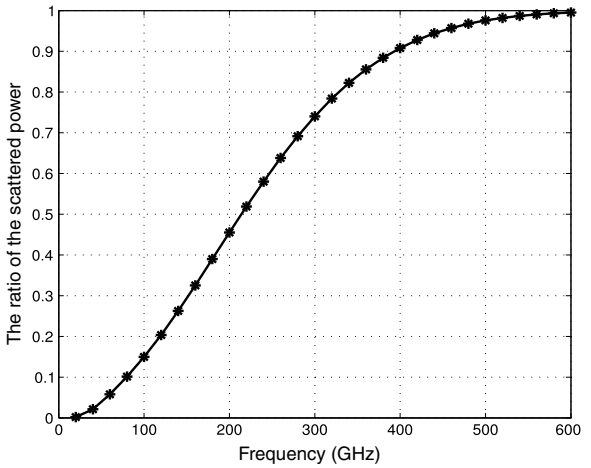

Fig. 5. The ratio of the scattered power to the total power. The parameters are the same as in Fig. 4.

we use small sub-tiles, the surface can be divided into even more sub-tiles and the power has a smaller amplitude. Vice versa, a larger sub-tile size will result in fewer sub-tiles with larger amplitude. Fig. 4 shows the combination effect of the specular term and the diffuse scattering term in Eq. (4). The specular term has a very narrow peak around the specular reflection point with a relatively large amplitude. The diffuse scattering terms are much wider around the specular point, but with smaller amplitudes. In our model, the specular reflected power is constant with respect to different division methods. That means that independent of the size a sub-tile, the specular reflected power and the total scattered power are all constant. The total power arriving at the receiver is the summation of the specular reflection power and the power from all other possible sub-tiles. It is obvious that the size of the sub-tiles only slightly influences the precision of the total power. Fig. 5 shows the effect of frequency on the specular and diffuse scattered fields. The figure presents the ratio of the diffuse scattered power to the total received power. The total power is composed of the diffuse scattered power and the specular reflection power. As the frequency increases, the surface changes from smooth to very rough. Then more power is diffuse scattered and the specular reflection power is no longer dominating. As a result, the ratio of the diffuse scattered power to the total power increases from very low to unity.

3. System model

3.1. The MIMO system model in the GHz band

Consider a MIMO system with N_t transmitting antennas and N_r receiving antennas, and suppose that both transmit and receive arrays are uniform linear arrays (ULAs). The channel matrix $\mathbf{H}$ is the summation of N multipaths as shown in Fig. 6. The discrete-time response of the channel can be written as

$$\mathbf{H} = \sum_{i=1}^{N} \beta_i \mathbf{e}_r(\Omega_{ri}) \mathbf{e}_t^*(\Omega_{ti}), \tag{11}$$

where β_i is the complex gain of the ith path, Ω_{ri} and Ω_{ti} are angles of arrival and departure of the ith path, respectively, $\mathbf{e}_r(\Omega_{ri})$ and $\mathbf{e}_t(\Omega_{ti})$ are the receive and transmit array response vectors, respectively [15, p. 349], and the asterisk denotes conjugate transposed. In a rich scattering environment, many independent rays exist in the channel. Statistically, in the GHz band, the amplitude of each ray is random, and the phase is uniformly distributed between 0 and 2π. Therefore, β_i are i.i.d. complex random variables with zero mean and unit variance. From the structure of $\mathbf{H}$, we know that with only one path (line of sight or a single reflected ray) between the transmitter and the receiver, a MIMO channel provides only a power gain but no degree of freedom gain [15, p. 351], because the channel coefficients are highly dependent, and the rank of $\mathbf{H}$ is 1. When multipaths exist, the signals from different paths can be regarded as from virtual "relays" which are geographically far apart. Therefore, a MIMO system can have multiplexing gain when the rays have different departure/arrival angles [15, p. 363]. However, the degree of freedom gain cannot exceed the number of multipaths. It is useless to utilize too many antennas if there are not enough scatterers in the channel. In fact, the channel may still be sparse under some conditions even if the MIMO scale is small, e.g., 8×8. Only when the number of multipaths is very large can the channel gains be regarded as Rayleigh distributed random variables. In this situation, the channel's degrees of freedom scale linearly with the channel dimension. In the GHz band, many models adopt this assumption. However, this is not the case in the THz band with smooth surfaces, as the number of multipaths are likely smaller than those in the GHz band.

3.2. The MIMO model in the THz band with rough surfaces

For the indoor channel, the multipaths originate from a few clusters, and each cluster is composed of many scattered rays. Based on the work of Saleh and Valenzuela [25], we propose a MIMO model in the THz band with rough surfaces. In this model, we assume the walls, ceiling, floor, and

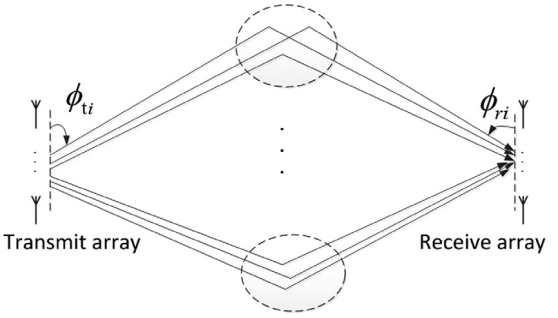

Fig. 6. MIMO model in a multipath environment.

large surfaces of furniture to be reflection surfaces. For the THz band, the number of clusters is usually small due to high path loss. As discussed in the previous section, each large surface results in many scattered sub-rays around the specular reflection point. The exact number of sub-rays is determined by the geometry of the room, the positions of antennas and the roughness of the surfaces. The impulse response of the THz channel can be written as

$$h(t) = \sum_{l=1}^{N_C} \sum_{k=1}^{N_L} \beta_{lk} \delta(t - T_l - \tau_{lk}), \tag{12}$$

where l represents the cluster number, k represents the sub-ray number in the cluster, and β_{lk} is the amplitude of each ray. T_l is the time delay of the lth cluster and τ_{lk} is the time delay of the kth ray in the lth cluster. In [17], the authors obtain the angular power profile by the ray-tracing method and experiments. Both results show that there are six main clusters and each of them has hundreds of multipaths, which validates our aforementioned statements.

Next we will determine the properties of clusters and sub-rays. In this paper, we assume the indoor scenario to be the same as in [17], using some large flat surfaces (walls or furniture) which act as reflection surfaces. On each large surface, a cluster of rays exists around the specular reflection point [17]. Note that in some other scenarios, for one reflection surface, the specular reflection ray might not exist and only diffuse scattering components are received. In our scenario, the angles of arrival/departure, the time of arrival and the normalized amplitude of each cluster in the THz band have the same distribution (normalized to the large scale fading path loss) as those at GHz frequencies. Unlike the statistical distribution of sub-rays in the GHz band, the sub-rays in each cluster at THz frequencies are determined, and can be obtained from the surface roughness theory. Here, we use the results in [26]. The amplitudes of the N_C first sub-rays in the N_C clusters follow the Rayleigh distribution, with a mean square value

$$\overline{\beta_{l0}^2} = \overline{\beta_{00}^2} e^{-T_l/\Gamma}, \tag{13}$$

where $\overline{\beta_{00}^2}$ is the mean power of the first ray in the first cluster, and Γ is the cluster decay parameter. As discussed in Section 2, the first sub-ray in each cluster is usually the ray with the largest power. For our indoor scenario, the specular reflection ray is the first sub-ray. We have not taken into consideration clusters without specular reflection rays as their power is very small. Note that $\overline{\beta_{l0}^2}$ is the power without considering the scattering coefficient. For a rough surface, the power of each sub-ray in the cluster can be obtained by multiplying each scattering coefficient with the first sub-ray. Mathematically, the power of the sub-rays is denoted as

$$\overline{\beta_{lk}^2} = \overline{\beta_{l0}^2} \langle \rho \rho^* \rangle_{lk} = \overline{\beta_{00}^2} e^{-T_l/\Gamma} \langle \rho \rho^* \rangle_{lk}, \tag{14}$$

where $\langle \rho \rho^* \rangle_{lk}$ is the average scattering power coefficient of the kth sub-ray in the lth cluster. In [21], the measured results coincide with the simulation results which validates the suitability of using a rough surface scattering model to obtain sub-rays in each cluster.

For the angles of arrival/departure of the clusters, a uniform distribution on the interval $[0, 2\pi)$ is a good fit for experimental results [26]. This also coincides with our intuition, as the reflection surface can be any part of the surface of a room. The ray angles within a cluster are not random. As shown in Fig. 3, the sub-rays all originate from the small sub-tiles, thus the angle of each sub-ray within a cluster is deterministic. Once the geometry is determined, the angles of arrival/departure can be calculated by the ray-tracing method. In fact, as we only consider single bounce rays, the angles of arrival are not independent of the angles of departure.

The time of arrival of clusters is described by a Poisson process. The distribution of the arrival time is given by

$$p(T_l | T_{l-1}) = \Lambda e^{-\Lambda(T_l - T_{l-1})}, \tag{15}$$

where Λ is the cluster arrival rate. The time of arrival of rays in each cluster can also be obtained by calculation. Therefore, τ_{kl} is fixed by the geometry of each ray.

The channel matrix $\mathbf{H}$ for the THz band has a form similar to Eq. (11), whose baseband equivalent model is written as

$$\mathbf{H} = \sum_{l=1}^{N_c} \sum_{k=1}^{N_l} \hat{\beta}_{lk} \mathbf{e}_r(\Omega_{rlk}) \mathbf{e}_t^*(\Omega_{tlk}) \tag{16}$$

where $\hat{\beta}_{lk}$ is the complex gain of the kth path in the lth cluster. The phase of $\hat{\beta}_{lk}$ is uniformly distributed between $[0, 2\pi)$, and the amplitude follows a Rayleigh distribution with a mean value of $\bar{\beta}_{lk}$. Note that the rays belong to several clusters, and the number of sub-rays in each cluster might not be the same. Based on this discussion, we reach the conclusion that the number of multipaths will influence the randomness of the channel matrix $\mathbf{H}$. When we have only a few clusters and each surface is smooth, there will be only a few rays, which results in the columns of $\mathbf{H}$ to be highly correlated.

3.3. The capacity of the MIMO channel in the THz band

The ergodic MIMO capacity is given by the following well-known formula

$$C = \mathbf{E}\left[\sum_{i=1}^{n_{\min}} \log_2\left(1 + \frac{P_i \lambda_i^2}{N_0}\right)\right] \text{ b/s/Hz}, \tag{17}$$

where $\mathbf{E}[\cdot]$ is the expectation, $n_{\min}$ is the rank of the random matrix $\mathbf{H}$, P_i is the transmit power of the ith stream, N_0

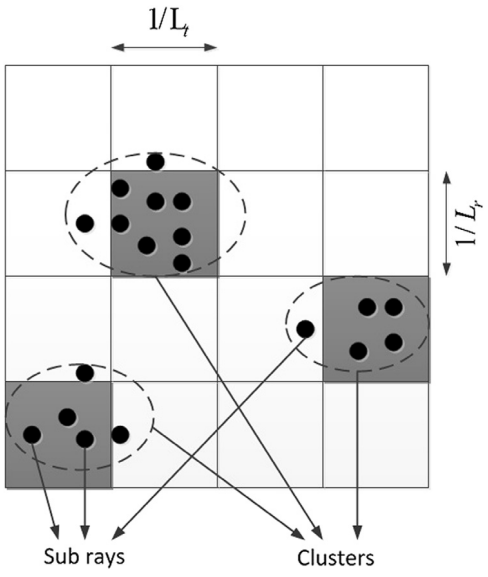

Fig. 7. Angular domain representation of the channel. Each square represents a resolution bin with a width of $1/L_r \times 1/L_t$. The shaded squares are the clusters and the dots are the sub-rays.

is the noise power spectral density, and $\lambda_1, \lambda_2, \ldots, \lambda_{n_{\min}}$ are the singular values of the random channel matrix $\mathbf{H}$. The capacity is influenced by the specular reflection ray and the scattered rays. When the surfaces are very smooth, the model reduces to that of GHz MIMO. In our model, there are fewer rays if the surfaces are very smooth, but the number of rays increases with surface roughness. Next we will analyze the MIMO capacity in the angular domain based on the work of Sayeed et al. [27–29].

Suppose all antennas are critically spaced at half the wavelength ($\Delta = 0.5$, where Δ is the receive antenna separation normalized to the carrier wavelength), $L_t = N_t\Delta$ and $L_r = N_r\Delta$ are the normalized lengths of the transmit and receive antenna arrays, respectively. From [15] we know that the system of N_r fixed vectors

$$\left\{\mathbf{e_r}(0), \mathbf{e_r}\left(\frac{1}{L_r}\right), \ldots, \mathbf{e_r}\left(\frac{N_r-1}{L_r}\right)\right\}, \tag{18}$$

can be one of the orthonormal basis sets for the received signal space. As the transmit antenna array has the same structure as the receive antenna array, the basis for the transmit signal space has exactly the same structure. Transforming the signals in the spatial domain into the angular domain, we can obtain the equivalent representation of the channel in the angular domain [15, p. 370]

$$\mathbf{H^a} = \mathbf{U_r^*} \mathbf{H} \mathbf{U_t}, \tag{19}$$

where $\mathbf{U_r}$ and $\mathbf{U_t}$ are the base of the received and transmit signal spaces taking the form of Eq. (18), with dimensions of $N_r \times N_r$ and $N_t \times N_t$, respectively.

Based on the previous discussion, we partition the physical paths into $L_r \times L_t$ resolvable bins, each with an angular width $\frac{1}{L_r} \times \frac{1}{L_t}$, as shown in Fig. 7. We project each ray into the angle lattice, and the results reveal the quality of the channel. For example, in [17], the authors measure the relative received power of different angles of arrival/departure reflected from moderately rough surfaces ($\sigma_h = 0.15$ mm and $f = 300$ GHz). Their figures show that there are several clusters randomly distributed on the lattice, and each cluster has a narrow angle spread. By observing the lattice structure (Fig. 7), we comment as follows:

- The amount of diversity equals the number of non-zero entries in the lattice, and the amount of degrees of freedom equals the amount of different angles. Since the THz MIMO channel in smooth surface (or slightly rough) environments usually has few clusters with narrow beams, both the diversity gain and the multiplexing gain are small, which results in a sparse MIMO channel. However, small scale MIMO systems usually have a full multiplexing gain.
- When the surfaces are rough, the beam reflected from one surface grows wider, and more resolution bins have sub-rays. Therefore, the rougher the surfaces, the more degrees of freedom the channel has. This will be shown in Fig. 8 in Section 4.
- The channel capacity of the MIMO system can be divided into two parts: one is for the specular, the other for scattering reflections. With the increase of surface roughness, the specular capacity will decrease while the scattering capacity will increase.
- The roughness of a surface can play a positive role in increasing the MIMO capacity in the THz band. When the surface is very smooth, there only exist few very strong specular reflection rays. A rough surface gives rise to many scattered rays in addition to the specular reflected rays. The power of each ray (specular or scattered) is smaller for rough surfaces than for smooth ones, yet the number of rays is much higher. As the multiplexing gain depends primarily on the angular spreads (the number of multipaths), and the power gain depends on the connectivity between the transmitting and receiving antennas (the power of rays), the roughness factor reduces the power gain but increases the multiplexing gain. Therefore, there may exist a tradeoff between the capacity and surface roughness.
- The surface roughness is especially essential for massive MIMO systems in the THz band. As the MIMO scale is extremely large and each resolvable bin is very narrow, only a few bins are non-zero if the surfaces are smooth. Therefore, the benefits of massive MIMO can be realized only with rough surfaces.

4. Results

In this section, we first study the distribution of the rays in clusters via Monte Carlo methods. Then we numerically evaluate the channel capacity with different roughness factors. Finally, the effect of different MIMO scales is analyzed.

4.1. Power distribution in the angular domain

In our simulations, we set the frequency to $f = 300$ GHz and select $\gamma = 20$ ns, $\Gamma = 60$ ns, and $\Lambda = 20$ ns. The distance between the transmitter and receiver is $r = 20$ m. The experimental results in [17] show that there are only

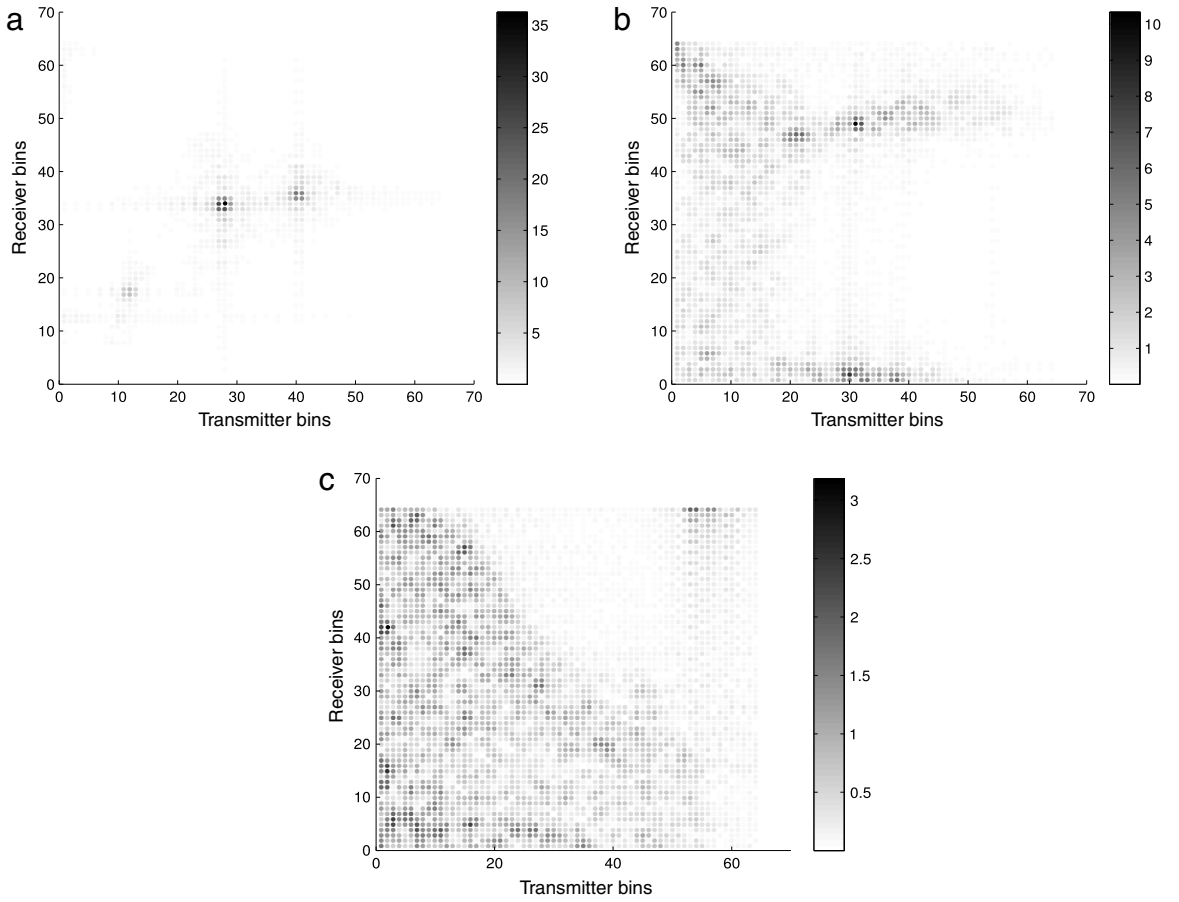

Fig. 8. Channel matrix in angular domain, with (a) $\sigma_h = 0.03$ mm, (b) $\sigma_h = 0.13$ mm, and (c) $\sigma_h = 0.23$ mm.

6–8 clusters in one simply decorated room. Therefore, we set the number of clusters as $N_c = 6$. In each cluster, we assume that the first sub-ray is the specular reflection ray which is reasonable for an indoor scenario [17]. The height deviations of the surfaces are $\sigma_h = 0.03$, 0.13 and 0.23 mm, and $l_x = l_y = 10T$ to get a higher precision. $T = 2.3$ mm, and $\sigma_h = 0.13$ mm are the parameters used in Fig. 4. The procedure of generating clusters is the same as in [26]. Once the clusters are determined, the sub-rays are generated by geometrical calculations.

Fig. 8(a) shows the power distribution in the angular domain with a surface height deviation of $\sigma_h = 0.03$ mm (g is in the order of 0.1). The MIMO scale is 64 × 64, and each dot represents one of the 4096 bins. This slight roughness can scatter the rays only in a narrow angle, and the specular reflection ray carries significantly higher power than the scattered rays. This coincides with our conclusion in Section 3.3. When the roughness increases to $\sigma_h = 0.13$ mm (g is in the order of 1) and $\sigma_h = 0.23$ mm (g is in the order of 10), the number of non-zero dots becomes larger while the amplitude of each ray reduces, as shown in Fig. 8(b) and (c).

4.2. Channel capacity analysis

The channel capacity for a 4 × 4 MIMO system with different surface roughness is shown in Fig. 9. Other

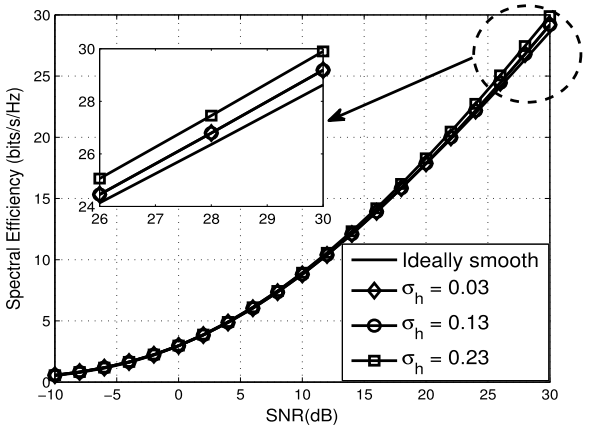

Fig. 9. The spectral efficiency of the 4 × 4 MIMO system. The parameters are the same as those in Fig. 4, with $\sigma_h = 0.03$, 0.13 and 0.23, respectively.

parameters are as in Fig. 8. The solid line, which is used as a benchmark, shows the spectral efficiency of a MIMO system with ideally smooth reflection surfaces. It is obtained by setting the roughness factor to zero while other parameters remain unchanged. The result agrees with that in [15, p. 400]. The dashed line shows the spectral efficiency of a system with the surface height deviation of

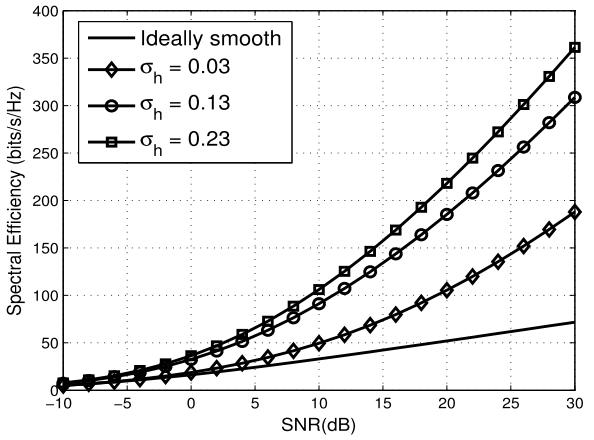

Fig. 10. The spectral efficiency of the 64 × 64 MIMO system. The parameters are the same as those in Fig. 4, with $\sigma_h = 0.03$, 0.13 and 0.23.

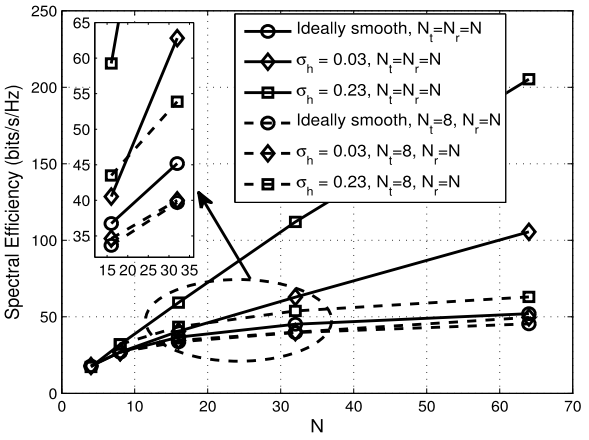

Fig. 11. The spectral efficiency of different MIMO scales. The *SNR* is 20 dB and the other parameters are the same as those in Fig. 4, with $\sigma_h = 0$, 0.03 and 0.23.

$\sigma_h = 0.03$ mm. The result is close to that with smooth surfaces. When the roughness increases to $\sigma_h = 0.13$ and $\sigma_h = 0.23$, the spectral efficiency is shown by the lines with circles and stars, respectively. Since the MIMO scale is relatively small, six clusters can provide full degrees of freedom; the spectral efficiency with rough surfaces is only slightly larger than that with smooth ones. Therefore, we can conclude that the roughness has little influence on the capacity of small scale MIMO systems in the THz band.

When the MIMO scale is large, however, we encounter a sparse fading channel due to the small number of clusters. Fig. 10 shows the capacity of a 64 × 64 MIMO system with other parameters is as in Fig. 9. Comparing the two solid lines in Fig. 10 and Fig. 9, we observe that more antennas contribute to a relatively small capacity increase in smooth environments. However, the capacity increase is obvious even when the surfaces are only slightly rough ($\sigma_h = 0.03$). When $\sigma_h = 0.13$ (the surface height deviation of some common materials are in this order), the capacity can be as high as 4–5 times of that with a smooth surface. If we further increase the roughness, the capacity continues to increase. This implies that rough surfaces are important in enlarging the capacity of large scale MIMO systems.

As discussed in Section 2, the roughness factor g is controlled by the deviation of surfaces σ_h, the incident/reflected angles and the frequency f. For the same surface, g quadratically increases with f according to Eq. (9). In the above simulations, we fixed the frequency at 300 GHz and obtained different results by varying σ_h. Obviously, once the environment is determined, different frequencies can introduce different spectral efficiency. Without considering large-scale fading, we can conclude from Fig. 10 that a higher frequency will result in higher spectral efficiency for large scale MIMO systems.

4.3. The importance of the MIMO scale

In this section, we analyze the significance of the MIMO scale. We examine two groups: an $N \times N$ and an $8 \times N$ scale. Other parameters are as in Fig. 8. In each group, the surface height deviation increases from ideally smooth to very rough. The spectral efficiency versus the MIMO scale N is shown in Fig. 11. The squared solid line shows the spectral efficiency with a very rough surface ($\sigma_h = 0.23$ mm). The line is almost linear which indicates that more antennas introduce higher degrees of freedom. When the surface is slightly rough ($\sigma_h = 0.03$ mm), the line is also linear with N but with a gentler slope, as shown by the diamond solid line. This means that only a portion of degrees of freedom is used under this scenario. The result for an ideally smooth surface is shown by the circled solid line. The spectral efficiency increases very slowly with the increase of N. For comparison, the dashed lines show the spectral efficiencies of the $8 \times N$ system. No matter how rough the surface is, the spectral efficiency increases only slowly with N. Note that, when the surface is ideally smooth, $N \times N$ and $8 \times N$ systems have almost the same spectral efficiency, which means that multiple antennas only provide power gain. Therefore, we can conclude that more transmitting antennas do not introduce multiplexing but only power gain when the surfaces are very smooth. Only with rough surfaces can we obtain the benefits from large scale MIMO systems.

5. Conclusion

A new MIMO system model for THz and nanocommunications is proposed that includes the effects of rough reflection surfaces. The results show that the MIMO channel in the THz band is very sparse if the reflecting surfaces are ideally smooth, and that with the increase of the MIMO scale, the sparsity becomes even more severe. When the surfaces are rough, the spectral efficiency of the MIMO system is higher than that with smooth surfaces, which is more pronounced with a larger MIMO scale. We show that surface roughness has a positive effect on increasing the spectral efficiency. Finally, numerical results on the performance of different MIMO scales reveal when it is necessary to use a large MIMO scale in the THz band. We hope that the results presented in this paper will aid future implementations of nanocommunication systems.

Acknowledgments

The authors would like to express their appreciation to Dr. Tao Lu of the University of Victoria for useful discussions on the reflection of electromagnetic waves from rough surfaces.

References

[1] R. Piesiewicz, M. Jacob, M. Koch, J. Schoebel, T. Kurner, Performance analysis of future multigigabit wireless communication systems at THz frequencies with highly directive antennas in realistic indoor environments, IEEE J. Sel. Top. Quantum Electron. 14 (2) (2008) 421–430.
[2] J.M. Jornet, I.F. Akyildiz, Graphene-based plasmonic nano-transceiver for terahertz band communication, in: Proc. 8th Eur. Conf. Antenn. Propag., 2014, pp. 684–688.
[3] J.M. Jornet, I.F. Akyildiz, Graphene-based nano-antennas for electromagnetic nanocommunications in the terahertz band, in: Proc. 4th Eur. Conf. Antenn. Propag., 2010, pp. 1–5.
[4] Y. Huang, L. Wu, M. Tang, J. Mao, Design of a beam reconfigurable THz antenna with graphene-based switchable high-impedance surface, IEEE Trans. Nanotechnol. 11 (4) (2012) 836–842.
[5] M. Tamagnone, J.S. Gomez-Diaz, J.R. Mosig, J. Perruisseau-Carrier, Reconfigurable terahertz plasmonic antenna concept using a graphene stack, Appl. Phys. Lett. 101 (2012) 214102.
[6] M. Dragoman, A.A. Muller, D. Dragoman, F. Coccetti, R. Plana, Terahertz antenna based on graphene, J. Appl. Phys. 107 (2010) 104313.
[7] I. Llatser, C. Kremers, D.N. Chigrin, J.M. Jornet, M.C. Lemme, A.C. Aparicio, E. Alarcon, Characterization of graphene-based nano-antennas in the terahertz band, in: Proc. 6th Eur. Conf. Antenn. Propag., 2012, pp. 194–198.
[8] Z. Xu, X. Dong, J. Bornemann, Spectral efficiency of carbon nanotube antenna based MIMO systems in the terahertz band, IEEE Wirel. Commun. Lett. 2 (6) (2013) 631–634.
[9] Z. Xu, X. Dong, J. Bornemann, Design of a reconfigurable MIMO system for THz communications based on graphene antennas, IEEE Trans. Terahertz Sci. Technol. 4 (5) (2014) 609–617.
[10] J.M. Jornet, I.F. Akyildiz, Channel modeling and capacity analysis for electromagnetic wireless nanonetworks in the terahertz band, IEEE Trans. Wireless Commun. 10 (10) (2011) 3211–3221.
[11] I.F. Akyildiz, J.M. Jornet, C. Han, Terahertz band: next frontier for wireless communications, Phys. Commun. 12 (2014) 16–32.
[12] K. Huang, Z. Wang, Terahertz terabit wireless communication, IEEE Microwave Mag. 12 (4) (2011) 108–116.
[13] H. Song, T. Nagatsuma, Present and future of terahertz communications, IEEE Trans. Terahertz Sci. Technol. 1 (1) (2011) 256–263.
[14] T.K. Ostmann, T. Nagatsuma, A review on terahertz communications research, J. Infrared Millim. Terahertz Waves 32 (2) (2011) 143–171.
[15] D. Tse, P. Viswanath, Fundamentals of Wireless Communication, Cambridge Univ. Press, Cambridge, UK, 2005.
[16] S. Priebe, C. Jastrow, M. Jacob, T.K. Ostmann, T. Schrader, T. Kurner, Channel and propagation measurements at 300 GHz, IEEE Trans. Antennas and Propagation 59 (5) (2011) 1688–1698.
[17] S. Priebe, M. Jacob, T. Kurner, AoA, AoD and ToA characteristics of scattered multipath clusters for THz indoor channel modeling, in: European Wireless, 2011, pp. 188–196.
[18] A. Sayeed, V. Raghavan, Maximizing MIMO capacity in sparse multipath with reconfigurable antenna arrays, IEEE J. Spec. Top. Signal Process. 1 (1) (2007) 156–166.
[19] V. Raghavan, G. Hariharan, A. Sayeed, Capacity of sparse multipath channels in the ultrawideband regime, IEEE J. Spec. Top. Signal Process. 1 (5) (2007) 357–371.
[20] W. Weichselberger, M. Herdin, H. Ozcelik, E. Bonek, A stochastic MIMO channel model with joint correlation of both link ends, IEEE Trans. Wireless Commun. 5 (1) (2006) 90–100.
[21] S. Priebe, M. Jacob, C. Jansen, T. Kurner, Non-specular scattering modeling for THz propagation simulations, in: Proc. 5th Eur. Conf. Antenn. Propag., 2011, pp. 1–5.
[22] R. Piesiewicz, C. Jansen, D. Mittleman, T.K. Ostmann, M. Koch, T. Kurner, Scattering analysis for the modeling of THz communication systems, IEEE Trans. Antennas and Propagation 55 (11) (2007) 3002–3009.
[23] C. Jansen, S. Priebe, C. Moller, M. Jacob, H. Dierke, M. Koch, T. Kurner, Diffuse scattering from rough surfaces in THz communication channels, IEEE Trans. Terahertz Sci. Technol. 1 (2) (2011) 462–472.
[24] P. Beckmann, A. Spizzichino, The Scattering of Electromagnetic Waves from Rough Surfaces, The Macmillan Company, New York, USA, 1963.
[25] A. Saleh, R. Valenzuela, A statistical model for indoor multipath propagation, IEEE J. Sel. Areas Commun. SAC-5 (2) (1987) 128–137.
[26] Q. Spencer, M. Rice, B. Jeffs, M. Jensen, A statistical model for angle of arrival in indoor multipath propagation, in: IEEE Proc. Veh. Technol. Conf., Vol. 3, 1997, pp. 1415–1419.
[27] A. Sayeed, Deconstructing multiantenna fading channels, IEEE Trans. Signal Process. 50 (10) (2002) 2563–2579.
[28] W. Bajwa, A. Sayeed, R. Nowak, Sparse multipath channels: modeling and estimation, in: Proc. 13th IEEE Digital Signal Processing Workshop, 2009, pp. 4–7.
[29] M. Matthaiou, A. Sayeed, J. Nossek, Sparse multipath MIMO channels: performance implications based on measurement data, in: Proc. IEEE 10th Workshop Signal Process. Adv. Commun., 2009, pp. 364–368.

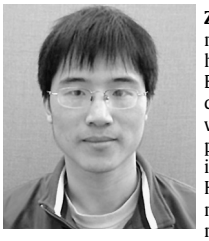

Zheng Xu received his B.Sc. degree in Telecommunication from Jilin University, China in 2008, his M.Sc. degree in Telecommunication from Beijing University of Posts and Telecommunications, Beijing, China in 2011. He is currently working towards the Ph.D. degree at the Department of Electrical and Computer Engineering, University of Victoria, Victoria, BC, Canada. His research interests include electromagnetic nanonetworks, graphene-based wireless communication, and terahertz band communication.

Xiaodai Dong received her B.Sc. degree in Information and Control Engineering from Xi'an Jiaotong University, China in 1992, her M.Sc. degree in Electrical Engineering from National University of Singapore in 1995 and her Ph.D. degree in Electrical and Computer Engineering from Queen's University, Kingston, ON, Canada in 2000. Since January 2005 she has been with the University of Victoria, Victoria, Canada, where she is now a Professor and Canada Research Chair (Tier II) at the Department of Electrical and Computer Engineering. Between 2002 and 2004, she was an Assistant Professor at the Department of Electrical and Computer Engineering, University of Alberta, Edmonton, AB, Canada. From 1999 to 2002, she was with Nortel Networks, Ottawa, ON, Canada and worked on the base transceiver design of the third-generation (3G) mobile communication systems.

She is an Editor for IEEE Transactions on Wireless Communications, IEEE Transactions on Vehicular Technology and Journal of Communications and Networks. Her research interests include communication theory, radio propagation, ultra-wideband radio, machine to machine communications, wireless security, smart grid, and signal processing for communication applications.

Jens Bornemann received the Dipl.-Ing. and the Dr.-Ing. degrees, both in Electrical Engineering, from the University of Bremen, Germany, in 1980 and 1984, respectively.

From 1984 to 1985, he was a consulting engineer. In 1985, he joined the University of Bremen, Germany, as an Assistant Professor. Since April 1988, he has been with the Department of Electrical and Computer Engineering, University of Victoria, Victoria, B.C., Canada, where he became a Professor in 1992. From 1992 to 1995, he was a Fellow of the British Columbia Advanced Systems Institute. In 1996, he was a Visiting Scientist at Spar Aerospace Limited (now MDA Space), Ste-Anne-de-Bellevue, Québec, Canada, and a Visiting Professor at the Microwave Department, University of Ulm, Germany. In 2003, he was a Visiting Professor at the Laboratory for Electromagnetic Fields and Microwave Electronics, ETH Zurich, Switzerland. From 1997 to 2002, he was a co-director of the Center for Advanced Materials and Related Technology (CAMTEC), University of Victoria. From 1999 to 2002, he served as an Associate Editor of the IEEE Transactions on Microwave Theory and Techniques in the area of Microwave Modeling and CAD. From 2006 to 2008, he was an Associate Editor of the International Journal

of Electronics and Communications. From 1999 to 2009, he served on the Technical Program Committee of the IEEE MTT-S International Microwave Symposium. He has coauthored Waveguide Components for Antenna Feed Systems—Theory and Design (Artech House, 1993) and has authored/coauthored more than 250 technical papers. His research activities include RF/wireless/microwave/millimeter-wave components and systems design, and field-theory-based modeling of integrated circuits, feed networks, ultra-wideband technology and antennas.

He is a Registered Professional Engineer in the Province of British Columbia, Canada. He is a Fellow IEEE, a Fellow of the Canadian Academy of Engineering (CAE) and serves on the editorial advisory board of International Journal of Numerical Modelling.